LATEST RESULTS FROM T
AT THE CERN $\bar{p}p$ COL

The UA2 Col
Bern, CERN, Copenhagen
Pavia, Saclay (CEN

PRESENTED BY A. I
CERN, Geneva,

ABSTR

Results obtained by the UA2 experim
of mass energy of 540 GeV are presented
properties of jets are described. Results
the jet system, on the parton density in t
distributions are reported. Measurement
in jets and the energy flow are given. T
$W/Z \rightarrow 2$ jets are presented.

The main results on the Z and the W
Low mass electron pairs are presented. A
photons is described. We report on the ob
characterized by the presence of a large tra
with missing energy and jet activity.

1. INTRODUCTION

We report data taken during two running periods in 1982 and 1983 with the UA2 apparatus. The apparatus is described in detail elsewhere.[1] It comprises two calorimeters. The central part, covering polar angles 40 to 140° consists of 240 towers, each segmented in an electromagnetic and two hadronic compartments.

The forward calorimeters (20 to 37.5 and 142.5 to 160°) consist of 240 electromagnetic cells each split in depth in two compartments of 24 and 6 radiation lengths. They are located after a toroidal magnetic field followed by a set of drift chambers to allow for the measurement of the charged particle momentum.

The interaction point is surrounded by a compact vertex detector to observe the charged particles produced in the $p\bar{p}$ collision and to measure the position of the event vertex. Both the central and the forward calorimeters are preceded by a preshower detector.

High p_T jets are detected with good quality in the acceptance of the central calorimeter, and with a poorer quality in the forward direction where the energy deposited in the electromagnetic calorimeters and the momentum of the charged particles measured in the magnetic spectrometers have to be combined.

High p_T electrons are detected in the polar angular range 20 to 120° and over the full azimuthal range. The electron signature requires an energy deposition in the calorimeters compatible with an electromagnetic shower, a matching charged track measured in the vertex detector aligned with a large signal observed in the preshower detectors. In the forward direction agreement between the momentum and the energy of the electron is required. The detection efficiency is about 77% for electrons while the rejection against jets is about 4×10^4.

We report results on jets from the 1983 data, corresponding to an integrated luminosity of 116 nb^{-1} and on events with electrons including the data from the 1982 data corresponding to a luminosity of 16 nb^{-1}.

2. TWO–JET PRODUCTION PROPERTIES

The recent unambiguous identification of jets in hadronic collisions[2,3] at the CERN $p\bar{p}$ Collider and at the ISR[4,5] has enabled a detailed study of the jet production and fragmentation properties. Inclusive jet production cross-sections from these data have been previously published[2] and were found to be in agreement with QCD predictions.

2.1 P_T OF THE TWO-JET SYSTEM

The intrinsic transverse momentum of the partons in the nucleon and the initial state gluon bremsstrahlung are expected to contribute to the transverse momentum p_T^{jj} of the two-jet system. Details of the results presented in Sections 2 and 3 can be found in Refs. 6-7.

Experimentally, p_T^{jj} is the vector sum of two large and opposite momenta and is therefore sensitive to instrumental effects. The two components p_η^{jj} (along the bisector of the two jets in the transverse plane) and p_ξ^{jj} (orthogonal to it and roughly parallel to the two-jet axis) are studied separately, because the effect of the detector resolution is much less on $|p_\eta^{jj}|$ than on $|p_\xi^{jj}|$. The rms of the two distributions shown in Figs. 1a and 1b are respectively 9.1 GeV for p_ξ^{jj} and 7.5 GeV for p_η^{jj}, with a negligible statistical error. Note however that the analysis criteria reject events with a very high value of p_T^{jj} and that instrumental effects contribute substantially to the measured widths of the p_ξ^{jj} distributions. In a perfect detector the widths of the p_ξ^{jj} and p_η^{jj} distributions are expected to be approximately equal.

The dashed lines in Fig. 1 show a QCD prediction.[8] To compare the prediction with the data, a complete Monte Carlo simulation, including all the detector details was performed. The corresponding distributions, shown as histograms in Fig. 1, are in good agreement with the experimental points. The result is sensitive to the assumption that gluons radiate more than quarks because of the

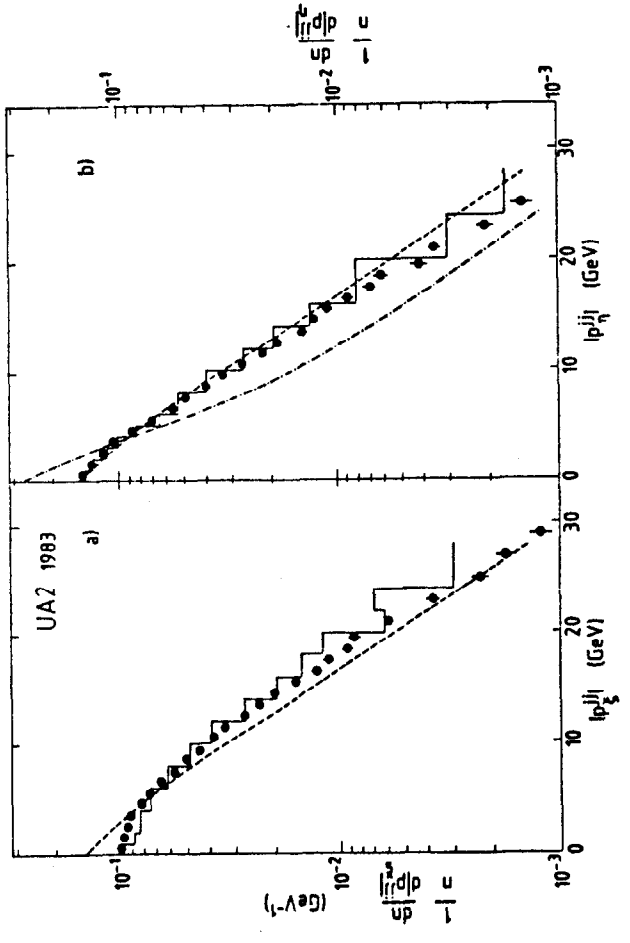

Fig. 1. Normalized distribution of the two jet transverse momentum, component perpendicular (a) and parallel (b) to the bisector of the two jet axis.

larger color charge of the gluon. As an example, the dashed-dotted line of Fig. 1b shows the distribution[8] expected in the case that gluons radiate like quarks.

2.2 FACTORIZATION

As was pointed out in Ref. 9 since all the QCD subprocesses involving a t-channel exchange of a vector boson give rise to a similar cms angular distribution, in lowest order QCD the jet cross section is expected to approximately factorize into an overall structure function $F(x)$ (sum of all the quark and gluon densities) and an effective parton-parton cross-section $d\sigma/d\cos\theta^*$, obtained from a weighted average over all the elementary subprocesses:

$$\frac{d^3\sigma}{dx_1 dx_2 d\cos\theta^*} = \frac{S(s_1,x_2)}{x_1 x_2}\,\frac{d\sigma}{d\cos\theta^*} = \frac{F(x_1)}{x_1}\,\frac{F(x_2)}{x_2}\,\frac{d\sigma}{d\cos\theta^*} \qquad (1)$$

where x_1 (x_2) represents the fraction of the longitudinal momentum carried by the interacting parton in the proton (antiproton). In the following analysis, higher order effects will be neglected ($K = 1$). The approximation of a small transverse momentum for the two-jet system, $p_T^{jj} \gg m_{jj}$, which is necessary to define θ^* without kinematical ambiguities,[10] has been shown to be reasonable in the previous section. This requirement is applied by retaining events only if they have $p_T^{jj} < 20$ GeV and $\Delta\phi_{jj} > 140°$.

As a first test of the factorization hypothesis the ratio of the distributions of the cms scattering angle $\cos\theta^*$ for two different intervals of jet-jet invariant mass is shown in Fig. 2a. As can be seen from Fig. 2a this ratio is consistent with unity as expected if factorization holds. As a further test, the factorization in x_1 and x_2 is tested by plotting the ratio $S(x_1,\ x_2)/S(x_1,\ x_2+\Delta x)$ as a function of x_1 for different intervals of x_2 (see Fig. 2b). For each interval of x_2 the ratio is independent of x_1 in agreement with the factorization hypothesis.

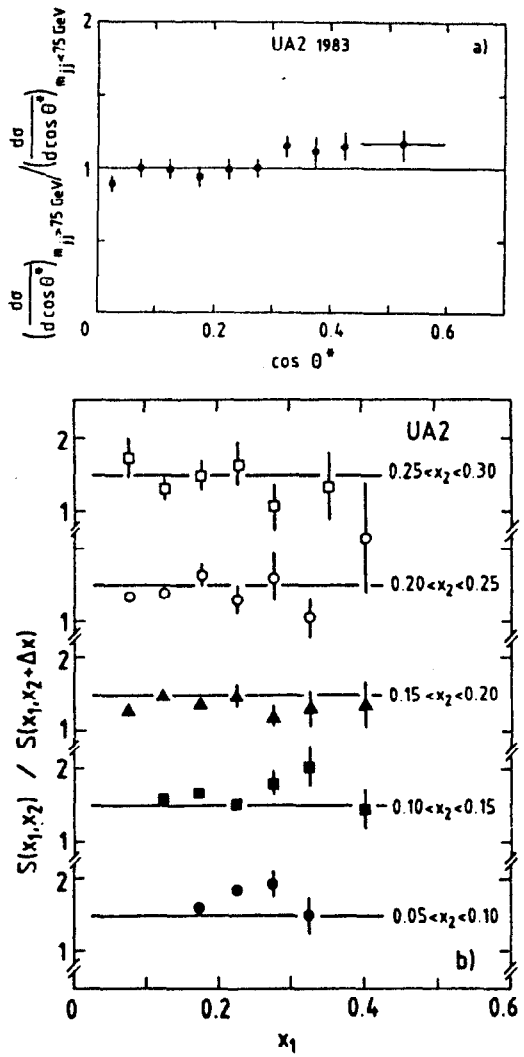

Fig. 2. a) Ratio between the angular distribution of the sample of events with $m_{jj} > 75$ GeV/c^2 and the events with $m_{jj} < 75$ GeV/c^2. b) Ratio $S(x_1, x_2)/S(x_1, x_2 + \Delta x)$ (see Eq. (1) in the text) for different x_2 slices and $\Delta x = 0.05$. The horizontal lines correspond to the slope of $F(x)$.

2.3 CMS Angular Distributions

The $d\sigma/d\cos\theta^*$ distribution is computed by considering the event distribution and taking into account the calorimeter acceptance. The overall normalization is chosen by arbitrarily setting the data point at $\cos\theta^* = 0$ equal to 1. The results are shown in Fig. 3. The systematic uncertainties which depend on the calorimeter acceptance are included in the errors. The systematic uncertainties due to the $\cos\theta^*$ resolution (≤ 0.04, independent of $\cos\theta^*$) and to the definitions of the kinematical variables adopted in this analysis are estimated to be $< 5\%$. In the region of overlap, the data agree well with the results of the UA1 Collaboration,[11] to within the statistical and systematic errors.

The observed angular distribution can be compared with the predictions of different theories. For example scalar gluon theories are clearly excluded.[12] The observed distribution is compared in Fig. 3 with the QCD prediction for the dominant parton-parton subprocesses[13] which lie in the area between the two dashed lines. The statistical and systematic errors are such that the relative importance of the different subprocesses cannot be measured. An overall QCD prediction, obtained from a sum of all the subprocesses, each weighted by a factor depending on the structure functions, gives good agreement. This curve is shown as a full line normalized to the data.

2.4 Structure Functions

The effective structure function $F(x)$ is evaluated according to Eq. (1) for 10 bins of x between 0.05 and 0.60. The effects of the resolution in x and of the variation of the acceptance as a function of the vertex position have been taken into account. If the usual definition of the higher order correction factor K were adopted, the result of the measurement would be the product $\sqrt{K} \cdot F(x)$. The result is shown in Fig. 4. An empirical fit (shown as a full line in Fig. 4) of the form $F(x) = Ae^{-\alpha x}$ gives $A = 6.2 \pm 0.1$ and $\alpha = 8.3 \pm 0.1$. The systematic errors,

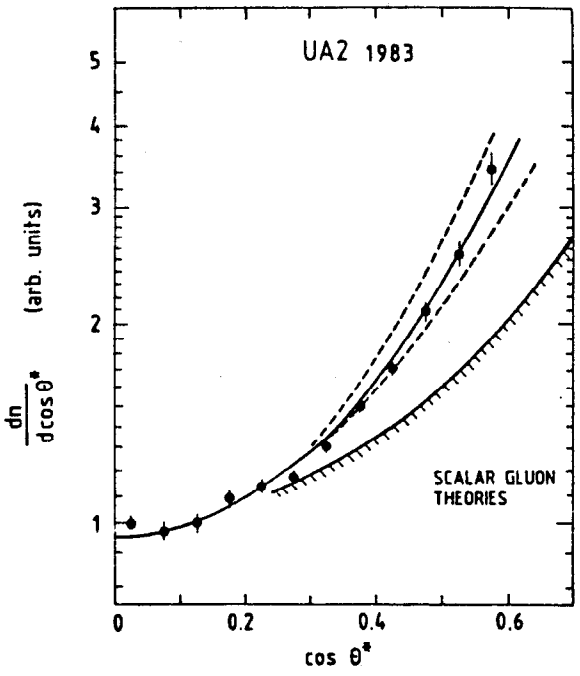

Fig. 3. Distribution of the scattering angle in the two-jet center of mass.

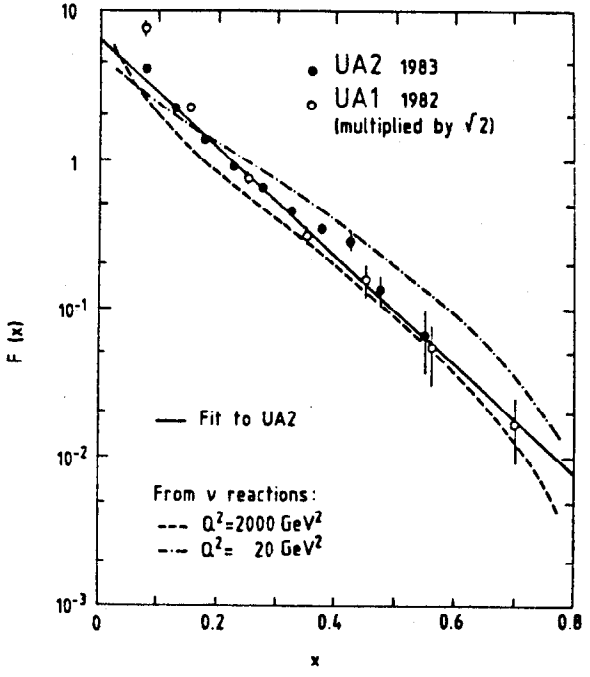

Fig. 4. Effective structure function.

due to the resolution, to the definition of the kinematics and to the uncertainty on the luminosity, are ±30%.

The structure function agrees with the one reported in Ref. 11 in the region $x \geq 0.10$, to within the statistical and systematic uncertainties. Since that analysis assumed $K = 2$, those points (shown in Fig. 4) have been multiplied by $\sqrt{2}$.

The parton density of Ref. 14, extrapolated to collider energies ($Q^2 = 2000$ GeV^2), is shown in Fig. 4 as a dashed line.

This structure function has been calculated assuming $F(x) = g(x) + 4/9\, q(x)$, where $g(x)$ is the gluon structure function and $q(x)$ is the sum over all the quark and antiquark densities. Part of the overall scale factor (≈ 1.4) may be attributed to higher order corrections, not taken into account in the computation of $F(x)$. The two distributions agree well in shape both in the region of small x (where $F(x)$ is dominated by the gluon density) and of high x, where mainly valence quarks are present.

3. FRAGMENTATION PROPERTIES

From the results on structure functions presented above, the jets in this energy range should be mixtures of quarks and gluons. It is therefore interesting to compare these jets with quark jets from e^+e^- data. According to QCD inspired models,[15-16] gluon jets are expected to fragment differently because of the larger color charge of the gluon. Results are presented on the charged particle multiplicity in jets and on the transverse energy flow in two-jet events.

3.1 Charged Particle Multiplicity in Jets

The charged particle multiplicity in jets was measured using the vertex detector. The analysis is restricted to the transverse plane where the track reconstruction efficiency is highest and where particles not associated with a jet are expected to contribute a uniform azimuthal distribution. Distributions of the azimuthal separation $\Delta\phi$ between all transverse tracks observed in the vertex detector and the energy centroid of the cluster having the highest transverse energy are shown in Fig. 5 for 2 intervals of m_{jj}. There are two peaks at $\Delta\phi \simeq 0$ and $\Delta\phi \simeq \pi$ as expected for two-jet events.

There is no unique way to define the charged particle multiplicity of jets produced in $\bar{p}p$ collisions because the relative fractions of the particles coming from the jet and coming from the "underlying event" (the part of the event which is due to the spectator parton fragments) are unknown. As a lower limit on the true jet multiplicity one can define the "jet core" multiplicity as the number of charged particles above a flat level corresponding to the value at $\Delta\phi = \pi/2$ (see Fig. 5): The data were corrected for detector inefficiencies and for γ conversions and π^0 Dalitz decays (the effect of this correction was 2%).

The corrected jet core multiplicities $\langle n_{ch}^{jet} \rangle$ are shown as a function of m_{jj} in Fig. 6. The error bars shown include a common 5% statistical uncertainty in the estimate of the two track resolution loss. The systematic error is estimated to be $\approx$ 15%. The dominant source of systematic error comes from the uncertainty in the two track resolution correction. The systematic error is mainly an overall scale error and the point to point systematic errors are much smaller.

Using the measured angular distributions of charged particles around the jet axis from e^+e^- data[17] the equivalent jet core multiplicity was evaluated for e^+e^- data by making a subtraction corresponding to the flat level at $\Delta\phi = \pi/2$. The results from the TASSO experiment are also shown in Fig. 6. The result suggests that jets from $\bar{p}p$ collisions in the mass range $40 < m_{jj} < 80$ GeV/c^2 have higher mean multiplicities than one would expect from extrapolations of e^+e^- data. In

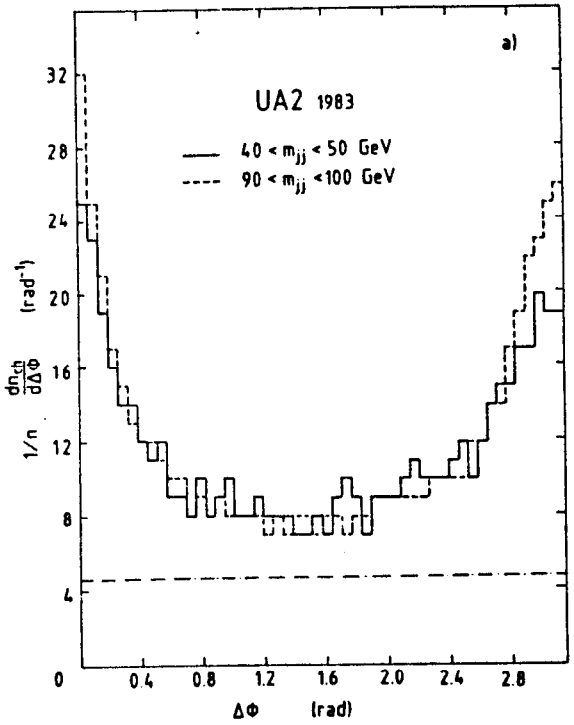

Fig. 5. Azimuthal separation $\Delta\phi$ between the energy cluster centroid of the leading jet and all charged transverse tracks, normalized to n, the number of events.

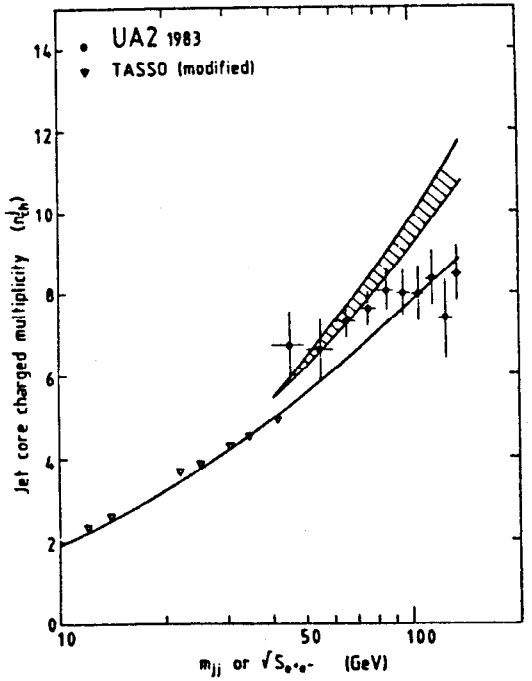

Fig. 6. Mean charged "jet core" multiplicities n_{ch}^{jet} as a function of $\sqrt{s_{e^+e^-}}$ for e^+e^- data and of the invariant two-jet mass m_{jj} for $\bar{p}p$.

order to understand this effect in more detail, the QCD parton shower model of Ref. 10 was used to predict the growth of multiplicity with m_{jj} for quark-antiquark (qq) (full line) and gluon-gluon (gg) jets (shaded area). The model for quark jets has been tuned to agree with e^+e^- data and therefore provides a good model for the extrapolation of e^+e^- data. The model also predicts the relative multiplicities of gluon jets compared to quark jets. Using the structure functions of Ref. 15 which are consistent with the ones measured in this experiment (see Section 2), one expects that the fraction of gluon jets varies from $\approx$ 75% to $\approx$ 30% as m_{jj} varies from 40 to 140 GeV/c^2. Allowing for this variation in the gluon fraction, the data are in agreement with the expectations of the model.

3.2 Energy Flow

The transverse energy flow around the jet axis was measured for a clean sample of two-jet events. To reduce the energy leaking outside the calorimeter acceptance, only clusters having a pseudorapidity, $|\eta|$, less than 0.3 (central clusters) are considered in this analysis. The distribution of the azimuthal transverse energy density $dE_T/d\Delta\phi$, integrated over a rapidity interval of ± 0.7 units around this central cluster is shown in Fig. 7 for three different intervals of the cluster transverse energy (E_T^j). The peaking in the energy flow is much stronger than in the charged particle flow (note the logarithmic scale in Fig. 7). The data are not corrected for the effects of calorimeter granularity and resolution. The main effect arises from the finite cell size ($\Delta\phi \times \Delta\theta = 15° \times 10°$) which tends to smear out the peaks. To compare the data with different fragmentation models, several Monte Carlo calculations were made. All details of the detector response were simulated for samples of events generated according to these models. The Monte Carlo event sample was submitted to the same trigger and analysis procedure as the real data.

The corresponding distributions are shown as smooth curves in Fig. 7. The Field-Feynman fragmentation model[18] with a rms transverse momentum of particles with respect to the jet axis, q_T, set equal to 350 MeV produces jets which are

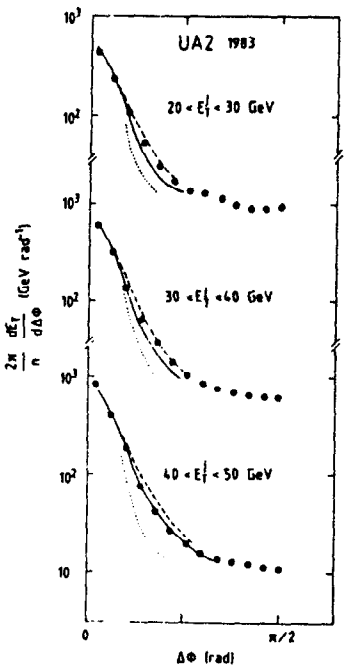

Fig. 7. Distribution of the azimuthal transverse energy density $dE_T/d\Delta\phi$ where $\Delta\phi$ is measured with respect to the centroid of the central cluster ($|\eta| < 0.3$).

much narrower than the data (dotted curve). The data can be better reproduced by models which include explicitly the effects of gluon bremsstrahlung, such as that used in Section 3.1. The data are bracketed by the predictions for qg and gg (solid and dashed curves) as expected for a mixture of quark and gluon jets.

4. TWO-JET MASS DISTRIBUTION

The dominant decay modes of the W and Z bosons are expected to result in two final-state jets. Therefore it is interesting to look for structure in the invariant two-jet mass distribution. It is important to optimize the mass resolution because of the large continuum QCD background. A sample of clean events with two jets in the central calorimeter and not too much energy in the forward-backward calorimeter were selected. For each event the energy of the second of the two jets is increased to balance the transverse energy of the first jet ($p_T^{jj} = 0$). The estimated mass resolution at a mass around 80 GeV/c^2 is 10 GeV/c^2. The normal threshold data were only used for invariant two-jet masses, m_{jj}, above 64 GeV/c^2 where there is no trigger bias. For the mass range $m_{jj} > 52$ GeV/c^2 the low threshold data was used and was allowed to have a free normalization in the fits. A first fit was made to the background region excluding the W and Z mass region ($66 < m_{jj} < 98$ GeV/c^2) of the form

$$d\sigma/dm_{jj} = Ae^{-\alpha m_{jj}} + Be^{-\beta m_{jj}} . \qquad (2)$$

Although there was no significant excess of events above the background a further fit was made over the full range, now including two Gaussian curves to allow for any contribution from W and Z decays into two jets. The background curve was fixed to the previous background fit. The ratio of Z^0 to W yields was fixed at 0.41 ($N_{tot} = N_W + N_Z$; $N_Z = 0.41 N_W$) and the ratio of masses was fixed at 1.15 as expected from the standard model. The resolution was fixed at 10 GeV/c^2. The result of the fit (see Fig. 8) was $N_W = 108 \pm 70$ and $M_W = 75 \pm 10$ GeV/c^2. Using the measured cross-section times branching ratio for $W \to e\nu$

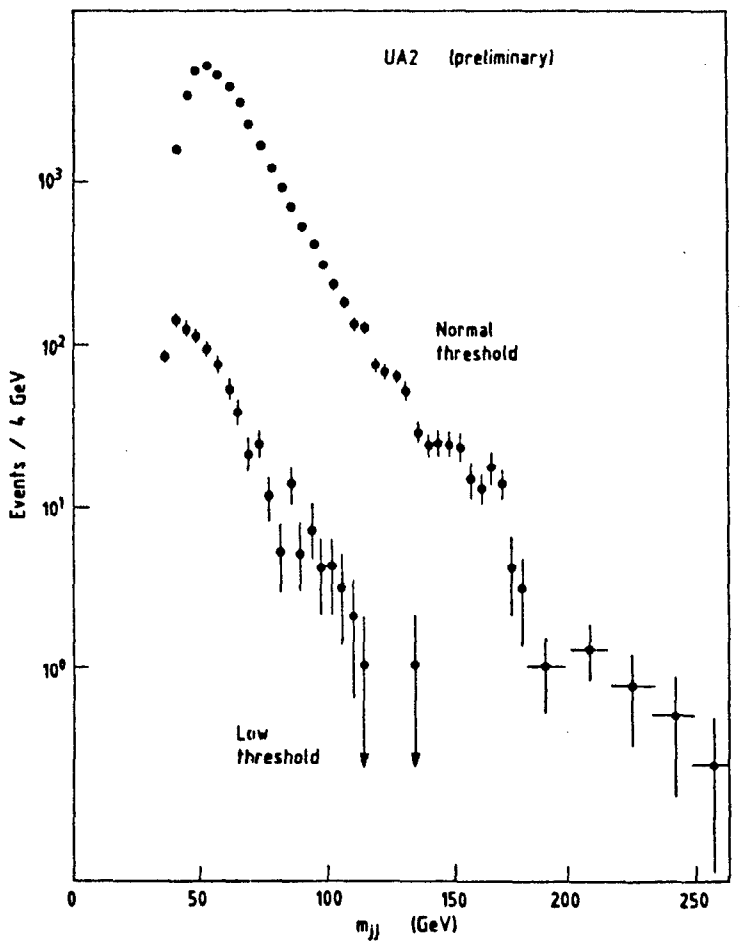

Fig. 8. Two-jet invariant mass distribution for normal and low threshold data.

decays[19-22] and the standard model prediction for the branching ratio of $W \to e\nu$, the expected value of $N_W \simeq 150$. Therefore the values of N_W and M_W are consistent with expectations. However since the value of N_W is not significantly different from zero it is clear that more data are needed. From the mass distribution (Fig. 8) there is some evidence for structure at $m_{jj} \approx 150$ GeV/c^2. To understand if this is statistically significant, further fits were made, after rebinning the data in the high mass region ($m_{jj} > 180$ GeV/c^2) so that all bins have a statistically significant content. Firstly, a pure background fit of the form of Eq. (2) was made which gave $\chi^2/ndf = 40/27$. Secondly, a fit was made with a free background of the form of Eq. (2) and a free Gaussian. The result of the fit (shown in Fig. 9) has 69 ± 17 events in the enhancement at a mass of $M = 147 \pm 3$ GeV/c^2 (where the quoted error is purely statistical). The χ^2/ndf of the fit is 28/25. The statistical significance of the enhancement was evaluated by using a maximum likelihood fit. This was done for the pure background and background plus Gaussian curves. The results from these fits (see Fig. 10) were consistent with the results of the χ^2 fits. From the ratio of the likelihoods of the fits with and without the Gaussian, the probability that a statistical fluctuation could generate such a enhancement can be estimated[23] to be 0.5%. Clearly more data are needed to confirm this result.

5. RESULTS ON W AND Z DECAYS INTO LEPTONS

In recent publications[19-21] we have described the observation in $p\bar{p}$ collisions of the W and Z^0 bosons via their electron decay mode.

5.1 HIGH-P_T ELECTRON SAMPLE

Using the electron signature mentioned in the introduction, we have isolated a sample of 225 events with an electron candidate with $P_T^e > 15$ GeV/c. In addition to electrons this sample still contains fake electrons resulting from misidentified hadrons, or hadron jets. If the electron is genuine, the event must contain either

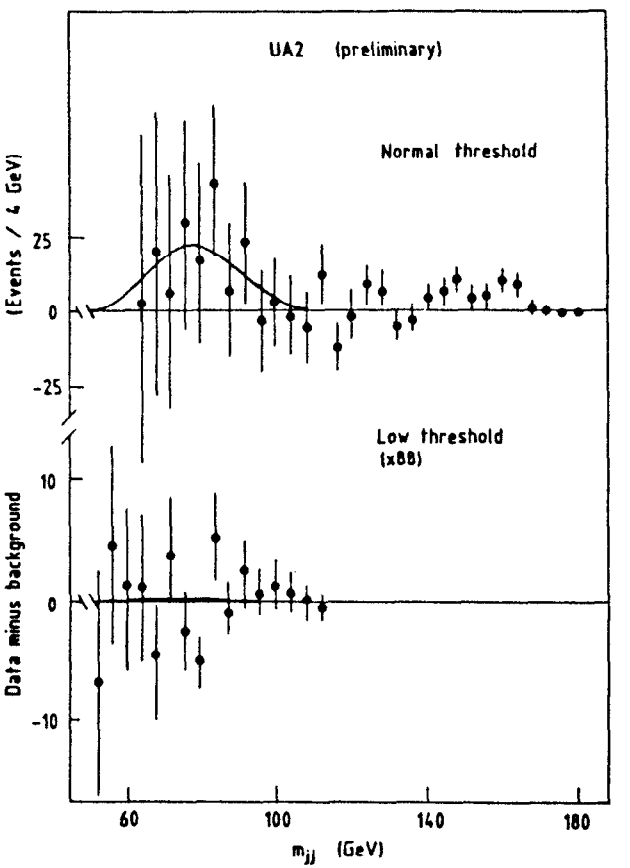

Fig. 9. Mass distribution showing the fit in the W mass region.

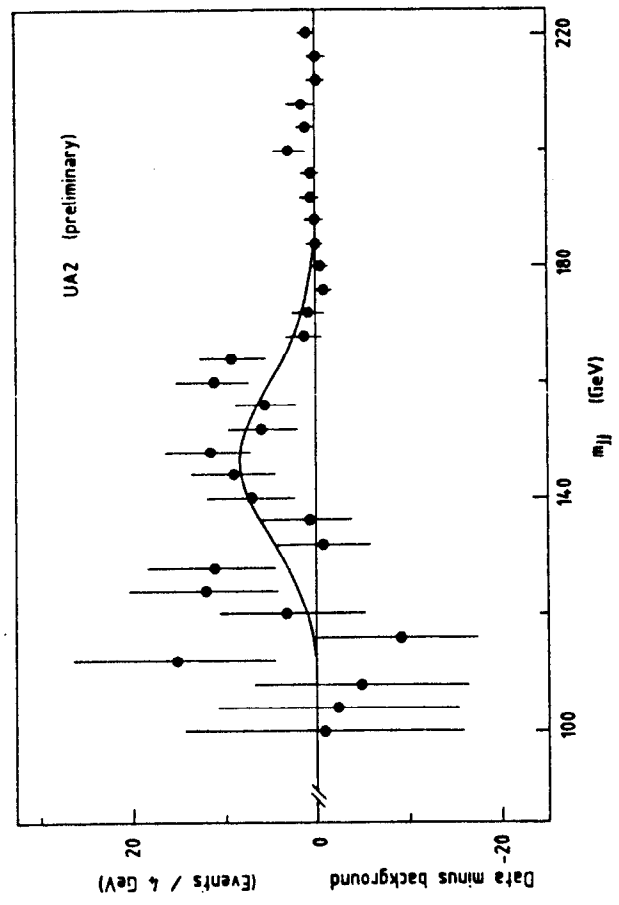

Fig. 10. Mass distribution showing the fit to the high mass region.

another electron of opposite charge, or a neutrino. However, if it is not genuine, we expect an additional jet at approximately opposite azimuth.[2] Forty-five events contain no jet (Fig. 11a). Events containing at least one jet ($P_T$jet > 3 GeV/c) fall into two classes : those with a jet back-to-back (Fig. 11b) which is dominantly background, and those in which the dominant jet activity is not back-to-back (Fig. 11c). Details of the selection criteria are described in Ref. 21 as well as the determination of the shape and magnitude of the background of misidentified hadrons, shown as solid lines in Fig. 11.

The combined P_T^e distributions of Fig. 11a and 11c show a characteristic Jacobian peak at $P_T^e \approx 40$ GeV/c, as expected from $W \to e\pm$ decay. Thirty seven events have $P_T^e > 25$ GeV/c with a background contamination of less than 1.5 events. These events have been used to determine the mass of the W and its production cross-section. The 8 shaded events in Fig. 11b are Z^0 decaying into e^+e^- pairs. They lead to the measurement of the Z^0 mass, width and production cross-section. Table 1 summarizes these measurements and the theoretical predictions.[24,25] This table shows the very good agreement of the masses with the theoretical predictions. Only the measured Z^0 cross-section is too large which leads to the amusing corrollary that the number of additional generation of light neutrinos $\Delta N_\nu < 0$ (2) with 90% (95%) confidence. This feature is not statistically significant, with the present limited sample. These results are also in good agreement with the UA1 measurements.[22,26]

Figure 12 shows the distribution of a measurement of the P_T of the W and Z^0, which can be large as expected from a full QCD treatment.[25]

The observation of one Z^0 event compatible with the decay $Z^0 \to e^+e^-\gamma$ and the observation of two similar events in the UA1 data[27] was unexpected. Using the UA2 event alone, we estimate a probability of 11% that at least one such event (with a configuration equal or less likely) should have resulted in our 8 event data sample from internal bremsstrahlung. Other estimation techniques give similarly large values. It is only with the combined results of UA1 and UA2

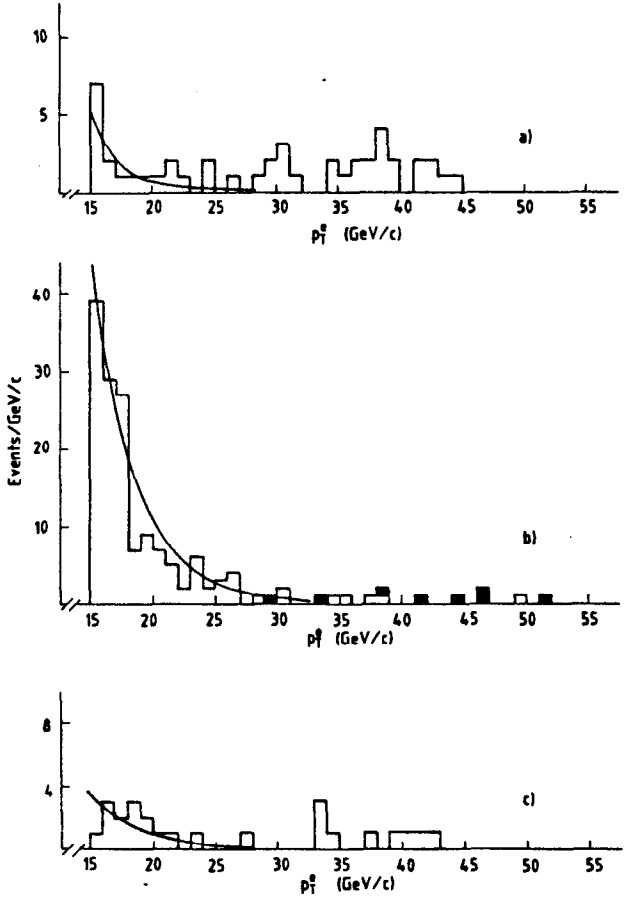

Fig. 11. Transverse momentum distribution of the electron candidates a) with no additional jets, b) with additional jets back-to-back in the transverse plane, and c) with additional jets not back to back.

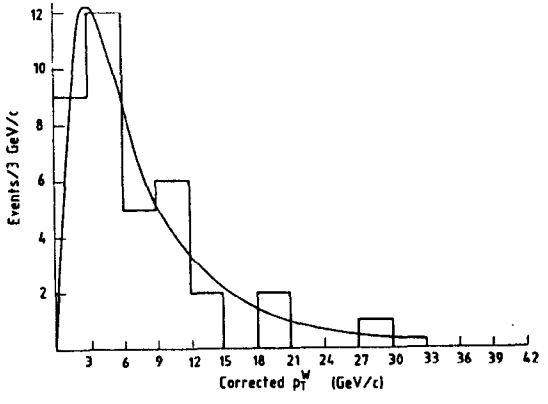

Fig. 12. Corrected p_T^W distribution. The curve represents a QCD prediction.

giving $2e^+e^-\gamma$ and $1\mu^+\mu^-\gamma$ events out of a sample of 17 Z^0 decays that the probablity of having at least such an unusual observation drops below 5%. In a search for such events in the W decays we have found one event with the electron and the photon collinear. It is not excluded that such an event results from the radiation of the electron in the vacuum chamber (4.5% probability).

Table 1

$W^\pm$ and Z^0 Properties;
(. . .) show predicted quantities[24,25]

	$W^\pm$	Z^0
Mass (GeV/c^2)	83.1 ± 1.9 (stat.) ± 1.6 (syst.) $\left(83.0^{+2.9}_{-2.7}\right)$	$92.7 \pm 1.7 \pm 1.4$ $\left(93.8^{+2.4}_{-2.2}\right)$
$\Gamma(W^\pm,\ Z^0 \rightarrow$ all) (GeV/c^2)	2.7 (assumed)	$< 6.5 \pm 0.6$ (90% CL)
σ^e (nb)	0.53 ± 0.1 (stat.) ± 0.1 (syst.) $\left(0.37^{+0.11}_{-0.06}\right)$	$0.11 \pm 0.04 \pm 0.02$ $\left(0.042^{+0.012}_{-0.006}\right)$
$\langle p_T \rangle$ (GeV/c)	6.9 ± 1.0	4.1 ± 1.3
$\sin^2\theta_W$	0.216 ± 0.01 (stat.) ± 0.01 (syst.) $[m_W = 38.65/\sin\theta_W]$ (0.217 ± 0.014)	

5.2 Associated Event Structure

For the W and Z^0 events, we have studied the system of all other observed particles in the event (the underlying event), after removing the associated electron(s) and jets (if any). Table 2 shows

i) the summed E_T of all other particles, $\sum \tilde{E}_T$,

ii) the probability for an event to have at least one associated jet of $E_T > 4$ GeV, and

iii) the associated mean transverse track multiplicity, n_T, and compares these results with minimum bias events, over the same rapidity range ($|\eta| < 1.7$).

Table 2

Associated Event Structure

	$W^\pm$	$W^\pm$ (no jet)	Z^0	Min. Bias
$\langle \sum \tilde{E}_T \rangle$ (GeV)	14.1 ± 1.7	9.7 ± 1.2	9 ± 2	8.8 ± 0.2
Probability ($E_T^J > 4$ GeV)	0.16 ± 0.07	–	0.13 ± 0.13	~ 0.07
$\langle n_T \rangle$	20.3 ± 2	15.3 ± 2	17.5 ± 3	14.7 ± 0.2

We note that the occurence of jets in the $W \rightarrow e\nu$ and $Z^0 \rightarrow e^+e^-$ samples is about twice that expected for minimum bias events. Otherwise, we find that the underlying event structure is similar to that of minimum bias events.

5.3 Low Mass Electron Pairs

Electron pairs are expected to result from Z^0 decay, and at lower mass from either the Drell-Yan mechanism or the semileptonic decay of heavy flavor. The latter category is expected to have associated jet activity.

We use a sample of events in which at least two isolated electrons of $p_T^e > 5$ GeV/c are identified. Data from the 1982 run were excluded from this study because of incomplete azimuthal coverage of the UA2 detector. This leaves an integrated luminosity of $\int \mathcal{L} dt = 116\ nb^{-1}$.

Figure 13 shows the low-mass electron pair spectrum with 8 $Z^0 \rightarrow e^+e^-$ events superimposed (4 events if the same data sample and selection criteria are used). Excluding Z^0 events, 13 events are measured in the mass range $12 < m_{ee} < 25$

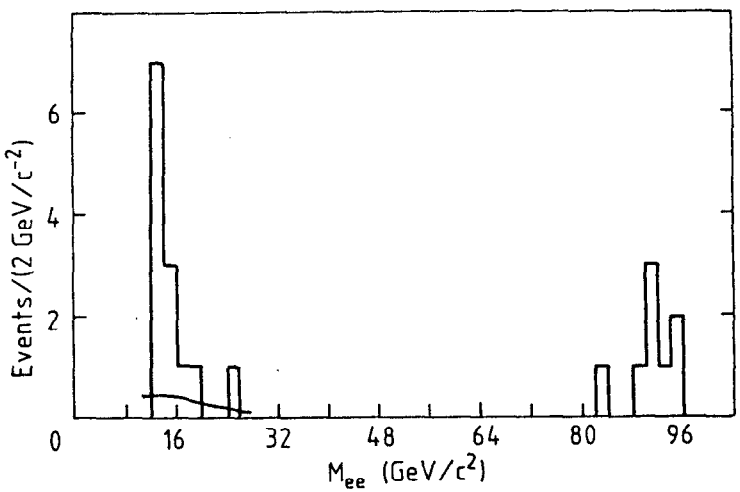

Fig. 13. Mass spectrum of low mass e^+e^- pairs. Identified $Z^0 \to e^+e^-$ decays have been superimposed. The curve is the estimated background to low mass e^+e^- pairs (2.4 ± 0.5 events).

GeV/c^2, implying, after acceptance corrections, an upper limit for the production of isolated pairs with mass $m_{ee} > 25$ GeV/c^2 of 130 pb (90% CL). Of these events, six events have associated jets nearby at least one electron. The relative contributions of events resulting from the Drell-Yan[28] process, and events resulting from the semileptonic decay of heavy flavors,[29] are being studied. After removing the electrons and associated jets, the underlying event structure has about twice the hadronic activity ($\langle \sum \tilde{E}_T \rangle$) of minimum bias events.

6. LARGE-E_T PHOTONS

Preliminary results were presented at this conference on an event with a single high p_T photon. This analysis has since been refined but should still be regarded as preliminary. Because of unknown background conditions associated with this event topology we analyze the data with the aim of placing upper limits on production cross-sections.

We select a sample of 205 events containing an isolated photon candidate of transverse energy $k_{T\gamma} > 15$ GeV. The candidates are characterized by a calorimeter energy deposition similar to that of high-p_T electrons, a signal in the preshower counters but no track within a 25° cone of the candidate direction.

The photons of this sample result from photons directly produced in the $p\bar{p}$ interaction, from the decay of produced particles (e.g. π^0 or multi-π^0 systems), or from a background of non-$p\bar{p}$ interactions.

The efficiency for genuine photon detection in the range $-0.7 < \eta < 0.7$ is $\approx$ 40%. This includes the probability for a photon to be converted in the preshower counter. The requirement of a signal in the preshower ensures that the background contamination from beam gas is small.

6.1 PHOTONS WITH LARGE MISSING TRANSVERSE MOMENTUM

Several models explaining the decay $Z^0 \to e^+e^-$ require decays of the type $Z^0 \to \nu\nu\gamma$, characterized by a single photon with large missing p_T. Excluding events with significant back-to-back jet activity (as expected from QCD processes), Fig. 14a shows the missing p_T of candidate photons. For $k_\gamma > 24$ GeV (that of the UA2 ($e^+e^-\gamma$) event), Fig. 14b shows the mean p_T of the event, excluding the photon, projected along the transverse γ-direction. Most events recoil in the transverse plane against the γ-direction. For Z^0 decays having a minimum-bias underlying event, we expect this distribution to peak around zero with a rms spread of 1.8 GeV/c. No event is consistent with $Z^0 \to \nu\nu\gamma$ (or even $\mu^+\mu^-\gamma$) for $k_\gamma > 24$ GeV. Assuming a phase space distribution for these decays this places an upper limit of 6 events.

More generally, we have searched for events characterized by a single jet with associated missing p_T. Only one event satisfying $p_T$miss > 50 GeV/c has been found. Above this missing-p_T value, the likelihood that one jet of a 2-jet event escapes detection is small. This event of 75 GeV/c missing p_T is characterized by a very electromagnetic energy deposition and no preshower signal so that it cannot be excluded as resulting from beam-halo background. At 90% confidence level, a limit of 53 pb can be placed on the cross-section production of monojets in ± 1 unit of rapidity.

6.2 PHOTON + ONE JET

A search has been made for photons accompanied by a jet (which may be back-to-back) of $E_T^j > 15$ GeV for evidence of high-mass objects. Figure 15a shows the (γj) mass spectrum, with a superimposed mass distribution of (multi-π^0, jets) normalized to the total photon sample. No significant clustering of events is observed. From the multi-π^0 distribution one expects only 0.1 event above 130 GeV. The 3 events observed might be explained by a single photon production.

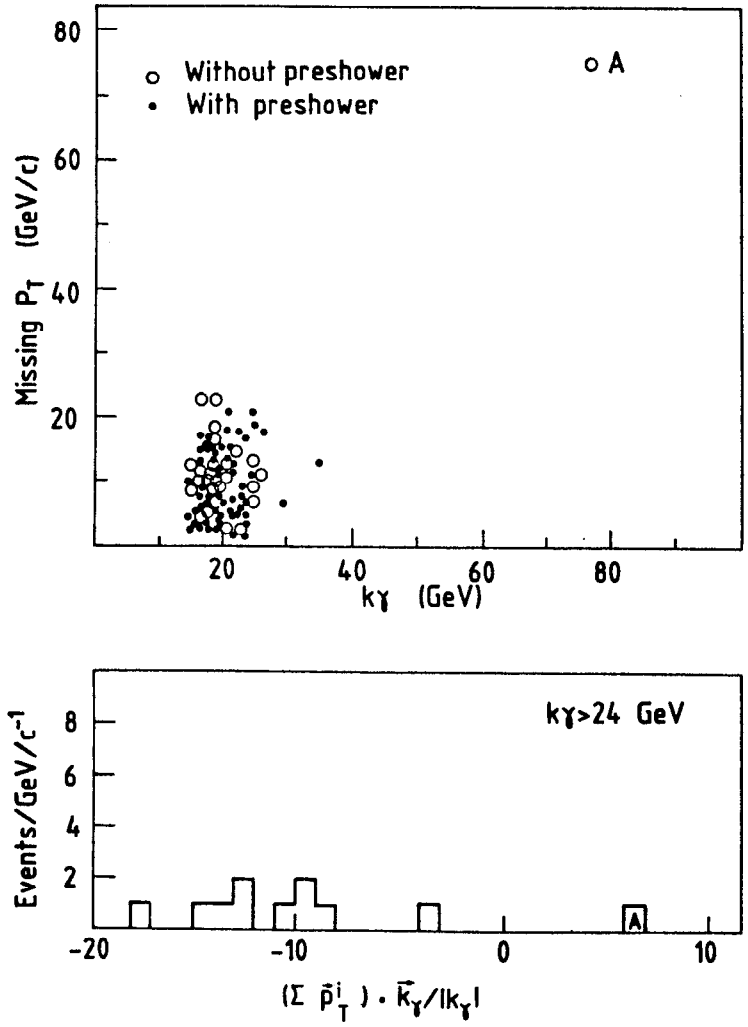

Fig. 14 a) Missing p_T of events containing a photon candidate of energy k_γ. b) Transverse momentum of the events after a cut $k_\gamma > 24$ GeV, after subtracting the photon candidate energy, projected in the transverse plane onto the photon direction.

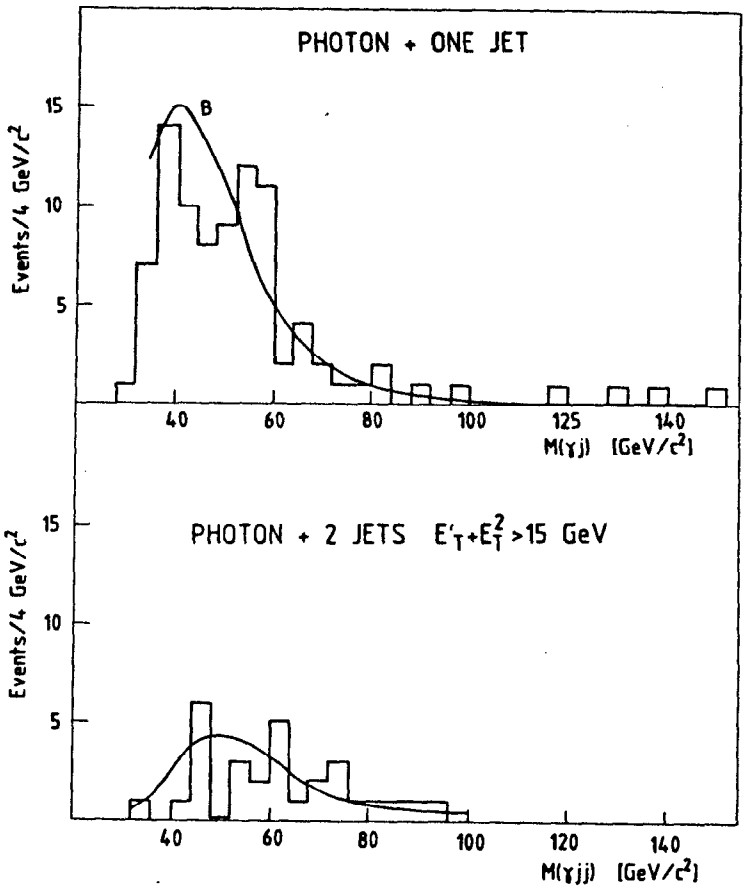

Fig. 15. a) Mass spectrum of events with a photon candidate of $k_\gamma > 15$ GeV, with 1 other jet of transverse energy $E_T(J) > 15$ GeV. b) As for Fig. 15a, but events for which the photon candidate is accompanied by two jets of summed $E_T[E_T^{j1} + E_T^{j2}] > 15$ GeV.

6.3 Photon + Two Jets

Figure 15b shows the $\gamma j^1 j^2$ mass spectrum for events with a photon candidate, and 2 jets satisfying $(E_T^{j1} + E_T^{j2}) > 15$ GeV. This search was motivated by the expectation that in composite or bound-state models, $Z^0 \to q\bar{q}\gamma$ decays should exist. No significant deviation from jet background is observed. This search places an upper limit of 20 events.

7. Events with Large p_T^e and Large p_T^ν

7.1 Observation of such events

From the sample of 225 events described in Section 5.1, we discard events collected in the 1982 period for which a wedge of 60° of the central calorimeter was removed to give room for a large angle magnetic spectrometer. We also discard 10 events in which the electron candidate is observed near the interface between the central region and one of the forward regions of the detector and is associated with nearby calorimeter energy in each of the two regions. The initial sample is reduced to 190 events, and the corresponding integrated luminosity to 116 nb^{-1}.

A large fraction of the 190 events have one or more jets. For each jet (j) we evaluate p_T^j and p_L^j, assuming the jet to be massless. We also evaluate $p_T(J)$ (the vector sum), $E_T(J)$ (the scalar sum) and $m(J)$ (the mass) for the system of all jets (J), or the system of jets and electrons (Je); $p_T(Je)$ measures the missing transverse momentum in the set of electrons plus detected jets with $E_T^j > 3$ GeV. The observation of large $p_T(Je)$ is generally equivalent to the presence of a neutrino, $p_T^\nu \approx p_T(Je)$. In this discussion 'neutrino' should be understood in the broad sense since the UA2 detector does not distinguish between a neutrino and any system of possible non-interacting paticles, such as photinos predicted by supersymmetric models. The distribution of $p_T(Je)$ is shown in Fig. 16a, where the superimposed background measures the probability that a multijet

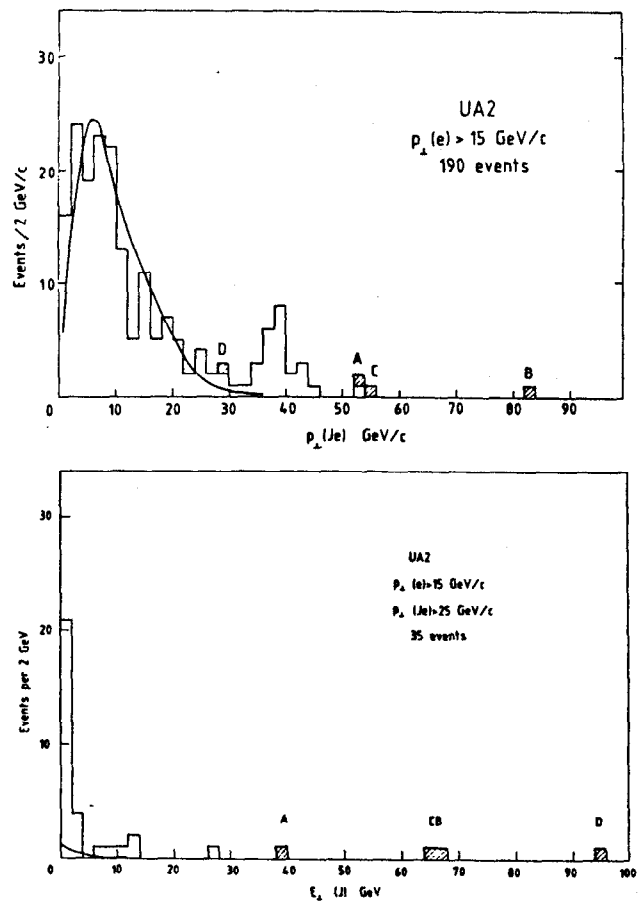

Fig. 16. a) Transverse momentum distribution of the system of electron and jets in the initial sample of 190 events. b) Transverse energy distribution of the system of jets in the sample of 35 events having $p_T(Je) > 25$ GeV. The event at $E_T(J) \approx 26$ GeV is the largest transverse momentum W in Fig. 8 of Ref. 21. The lines correspond to the calculated background contaminations.

event contains a misidentified electron and/or undetected jet(s) escaping the UA2 acceptance. The 35 events having $p_T(Je) > 25$ GeV/c have an estimated background of 3.4 ± 0.3 events.

For this sample of 35 events, Fig. 16b shows $E_T(J)$, the level of hadron activity in the event. The 31 events having $E_T(J) < 30$ GeV all belong to the W-event sample of Section 5 (Figs. 11c and 11c); four events ($A - D$) stand out above a background in the $[p_T(Je),\ E_T(J)]$ plane of 0.45 ± 0.04 events for $p_T(Je) > 25$ GeV/c and $E_T(J) > 30$ GeV (Fig. 17). We can evaluate the expected background contributions B_1 and B_2 for the following configurations:

$$B_1 : p_T(Je) > p_0,\ E_T(J) > 30 \text{ GeV} \quad \text{and}$$
$$B_2 : p_T(Je) > 25 \text{ GeV/c},\ E_T(J) > E_0 \ . \tag{3}$$

In each of the four events, either B_1 or B_2 is always less than 0.02. No background event exists in the region $p_T(Je) > 50$ GeV/c, $E_T(J) > 30$ GeV, which contains events A to C. We infer from this a background contamination of, at most, 0.02 events (90% confidence level) in this region.

In no event is there evidence of large p_T particles hitting passive detector elements, such as the magnet coils, in the azimuthal region where the neutrino is expected. However, event D has an azimuthal configuration similar to a two-jet event and this interpretation cannot be excluded.

In all events, the sharing of jet energies between the different calorimeter compartments is consistent with expectation. Also each jet has several tracks pointing to the vertex, making interpretations such as beam-gas background, or cosmic rays, unlikely.

A muon can in principle simulate a neutrino in the UA2 detector. We searched without success in each event for a track near the neutrino azimuth, and associated with calorimeter energy consistent with the response of a minimum ionizing particle.

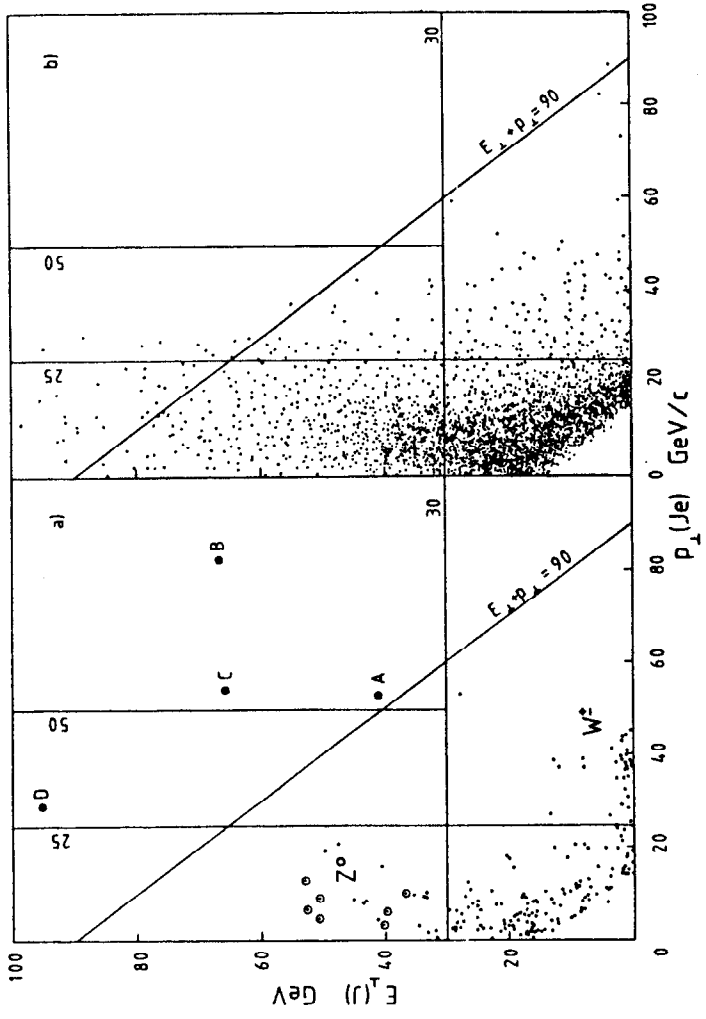

Fig. 17. a) Distribution of the 190 events of the initial sample in the $p_T(Je)$, $E_T(J)$ plane. b) Distribution of the background sample in the $p_T(Je)$, $E_T(J)$ plane. A reduction factor of 141 must be applied to infer from this sample the background contamination to the sample of Fig. 17a.

An event appearing at $(p_0,\ E_0)$ in the $p_T(Je)$, $E_T(J)$ plane (Fig. 17) may be interpreted as containing an undetected jet which would account, at least in part, for the measured value of p_0. If this jet had been detected, the same event would have appeared at $(p_0',\ E_0')$ with $p_0' < p_0$ and $p_0' + E_0' \geq p_0 + E_0$. But the only events having $p_T(Je) + E_T(J) > 90$ GeV are the events of Fig. 17. The absence of other events in this region, even with low values of $p_T(Je)$, makes that interpretation unlikely.

Figure 18 shows the transverse momentum configuration of each event.

7.2 Event Interpretation

Details of each event are listed in Table 1 of Ref. 30.

While events A to C have a large $(e\nu)$ azimuthal opening angle, that of event D is small. Since its minimum $(e\nu j_2)$ mass is 23 ± 6 GeV/c^2, and its associated $(e\nu j_1 j_2)$ mass is 145 ± 15 GeV/c^2, event D cannot be easily interpreted as resulting from W-decay. However, the configuration is suggestive of a $(q\bar{q})$ pair where one quark decays semileptonically. Because of the absence of other events of similar topology and because of its similarity to a two-jet event, we defer such an interpretation pending the observation of additional events of the same type.

The other events (A to C) have a transverse $(e\nu)$ mass of between 56 and 82 GeV/c^2, suggestive of $W \to e\nu$ decay. Choosing the minimum $|x_F(WJ)|$ which forces $m(e\nu) = m(W)$, the mass $m(WJ)$ of all three events is in the range $160 < m(WJ) < 180$ GeV/c^2. This may be kinematic in origin, since the background peaks in the same region.

If events A to C are interpreted as W-production with associated jet activity, their rate of occurence should be predicted by known QCD processes. Integrating over all event topologies, Minkowski[31] predicts less than 0.14 events to satisfy $p_T(W) > 40$ GeV/c. A more realistic upper limit should take into account the

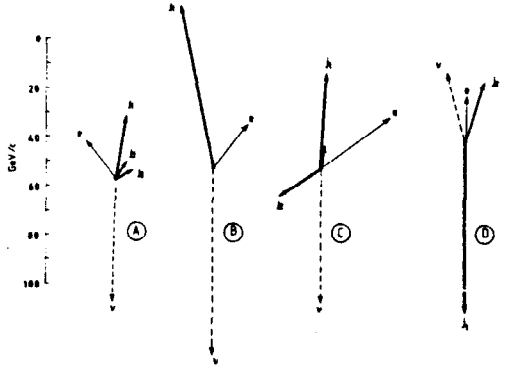

Fig. 18. Transverse momentum configuration of the four events having $p_T(Je) >$ 25 GeV/c and $E_T(J) > 30$ GeV. Their relative orientation is arbitrary.

topology of the events, and we consider

$$\frac{\sigma(p\bar{p}\to W + J + \ldots)}{\sigma(p\bar{p}\to W + \ldots)} \approx \frac{\sigma(p\bar{p}\to j_1 j_2 + J + \ldots)}{\sigma(p\bar{p}\to j_1 j_2 + \ldots)} \qquad (4)$$

where $j_1 j_2$ is a pair of jets having the same configuration as the $e\nu$ pair ascribed to a W decay. This relation holds approximately for processes in which $j_1 j_2$ couples via a gluon to a quark-antiquark pair (although the W-current, contrary to the gluon-current, is flavor changing). We expect the contribution of other QCD subprocesses, and interferences among them, to alter only slightly the right-hand side of the above relation. We evaluate such upper limits for events A to C from the sample of jet events. We take as J any jet (jet pair) having a tranverse momentum (invariant mass) at least as large as that of the corresponding jet (jet pair) in events A and B (C).

In our data sample, less than 0.4 events of the type of event A are expected; however, this event requires a W longitudinal momentum of $\approx$ 150 GeV/c to be interpreted as a $W\to e^{\pm}$ decay. The number of events like B and C, resulting from QCD processes, is less than 0.012, and 0.007 respectively, making their interpretation as W-jet(s) associated production from known processes unlikely. We should also expect events of the same type, with the $(e\nu)$ pair replaced by a $W\to j_1 j_2$ decay, with a higher rate. From our own data, this event topology cannot be excluded.

It is important to note that the (unlikely) interpretation of events A to C in terms of $W\to e\nu$ decay is not mandatory, and indeed the missing transverse energy may be shared by several undetected particles.

These events which include an electron, missing P_t and jets correspond to the topology expected from $W\to tb$ followed by the leptonic decay of the top quark $t\to e\nu b$. The momenta and masses of the 4 events A to D exclude their origin from such a decay. We have searched for events containing an electron and at least 2 jets of momenta larger than 9, 10 and 5 GeV/c respectively. We have found a few events satisfying these criteria. At such low p_T, the rejection against jets of the

electron signature is marginal so that the separation of top events from purely hadronic background having the same topology is difficult. We expect only about 1 top event identified in the UA2 detector for the integrated luminosity of 116 nb^{-1}.

8. CONCLUSIONS

We have given results on the production and fragmentation properties of jets. The quality of their agreement with the prediction from QCD calculation was shown.

A preliminary search for structure in the two-jet mass distribution showed no statistically significant evidence for $W/Z \rightarrow 2$ jets. There is some evidence for structure around $m_{jj} \approx 150$ GeV/c^2 although more data are needed to confirm this observation.

We have summarized the results on the production and decay into electron of the intermediate vector bosons W and Z and recalled the good agreement with the prediction of the $SU(2) \times U(1)$ theory.

We have found four events in which the $(e\nu)$ pair is produced in association with large-E_T jet(s) activity. Three of these events contain an $(e\nu)$ pair of large transverse mass, and we have attempted to describe them in terms of W-jet(s) associated production. Within the context of that hypothesis, at least two events are unlikely to result from known processes.

In a search for events involving a single jet we have found only one event with missing transverse energy in excess of 45 GeV. However, it cannot be excluded that this event results from beam-halo background.

The existence of $(Z^0 \rightarrow e^+e^-\gamma)$ decays was unexpected, and more data are needed to ascertain whether the rate of this process is consistent with internal bremsstrahlung.

We have searched for events with isolated photons. The results show no unexpected behavior.

Within the limited statistics so far available, other aspects of our data are generally as expected, but in many subjects, the need for more statistics is obvious.

REFERENCES

1. B. Mansoulié, The UA2 apparatus at the CERN $\bar{p}p$ Collider, *Proceedings 3rd Moriond Workshop on $\bar{p}p$ Physics*, editions Frontières, 1983, p. 609.
   M. Dialinas et al., The Vertex Detector of the UA2 Experiment, LAL-RT/83-14, ORSAY, 1983.
   C. Conta et al., The System of Forward-Backward Drift Chambers in the UA2 Detector, CERN-EP/83-176, submitted to Nucl. Instrum. Methods.
   K. Borer et al., Multitube Proportional Chambers for the Localization of Electromagnetic Showers in the UA2 Detector, CERN-EP/83-177, submitted to Nucl. Instrum. Methods.
   A. Beer et al., The Central Calorimeter of the UA2 Experiment at the CERN $\bar{p}p$ Collider, Nucl.Instrum. Methods. 224 (1984) 360.
2. UA2 Collaboration, M. Banner et al., Phys. Lett. 118B (1982) 203;
   UA2 Collaboration, P. Bagnaia et al., Z. Phys. C20 (1983) 117;
   UA2 Collaboration, P. Bagnaia et al., Phys. Lett. 138B (1984) 430.
3. UA1 Collaboration, G. Arnison et al., Phys. Lett. 123B (1983) 115.
4. Axial Field Spectrometer Collaboration, T.Åkesson et al., Phys. Lett. 118B (1982) 185 and 193.
5. COR Collaboration, A.L.S. Angelis et al., Phys. Lett. 126B (1983) 132.
6. UA2 Collaboration, P. Bagnaia et al., Phys. Lett. 144B (1984) 283.
7. UA2 Collaboration, P. Bagnaia et al., Phys. Lett. 144B (1984) 291.

8. M. Greco, Back-to-Back Jets as a Test of the Three Gluon Coupling, LNF preprint 84/21 (1984), submitted to Z. Phys. C.

9. G. Cohen-Tannoudji et al., Phys. Rev. D28 (1983) 1628;
B. L. Combridge and C. J. Maxwell, RL-83-095 (1983);
F. Halzen and P. Hoyer, Phys. Lett. 130B (1983) 326.

10. J. C. Collins and D. E. Soper, Phys. Rev. D16 (1977) 2219.

11. UA1 Collaboration, G. Arnison et al., Phys. Lett. 136B (1984) 294.

12. D. Drijard et al., Phys. Lett. 121B (1983) 433.

13. B. L. Combridge, J. Kripfganz and J. Ranft, Phys. Lett. 70B (1977) 234;
see also: R. Cutler and D. Sivers, Phys. Rev. D17 (1978) 196.

14. CDHS Collaboration, H. Abramowicz et al., Z. Phys. C12 (1982) 289; Z. Phys. C13 (1982) 199; Z. Phys. C17 (1983) 283 and H. Blümer, private communication.
See also the corresponding result from the CHARM Collaboration, F. Bergsma et al., Phys. Lett. 123B (1983) 269.

15. G. Sterman,S. Weinberg, Phys. Rev. Lett. 39 (1977) 1436;
K.Shizuya, S.-H.H. Tye, Phys. Rev. Lett 41 (1978) 787;
M.B. Einhorn, B.G. Weeks, Nucl. Phys. B146 (1978) 445.

16. G. Marchesini and B.R. Webber, Nucl. Phys. B238 (1984) 1.
B.R. Webber, Nucl. Phys. B238 (1984) 492.

17. TASSO Collaboration, M. Althoff et al., Z. Phys. C22 (1984) 307.

18. R.D. Field and R.P. Feynman, Nucl. Phys. B136 (1978) 1.

19. M. Banner et al., Phys. Lett. 122B (1983) 476.

20. P. Bagnaia et al., Phys. Lett. 129B (1983) 130.

21. P. Bagnaia et al., Z. Phys. C24 (1984) 1.

22. UA1 Collaboration, G. Arnison et al., Phys. Lett. 126B (1983) 398.

23. W. Eadie et al., *Statistical Methods in Experimental Physics*, 231, North-Holland 1971.

24. For a review, see W.J. Marciano, Weak Interactions, *Proc. Int. Symposium on Lepton and Photon Interactions at High Energies*, Ithaca, 1983 (Cornell Univ., Ithaca, NY, 1983), p.80.

25. G. Altarelli, R.K. Ellis, M. Greco and G. Martinelli, Vector Boson Production at Colliders: a Theoretical Reappraisal, preprint CERN-TH 3851 (1984).

26. G. Arnison et al., Phys. Lett. 122B (1983) 103;
G. Arnison et al., Phys. Lett. 129B (1983) 273.

27. G. Arnison et al., Phys. Lett. 135B (1984) 250.

28. S. Drell and T. Yan, Phys. Rev. 25 (1970) 316;
For a review, see G. Altarelli, Phys. Reports 81 (1982) 1.

29. E. Berger and D. Soper, CERN-TH/3850 (1984);
H. Fischer and W. Geist, Z. Phys. C19 (1983) 159;
S. Pakvasa et al., Phys. Rev. D20 (1979) 2862;
E. Glover, F. Halzen and A. Martin, Phys. Lett. 141B (1984) 429.

30. P. Bagnaia et al., Phys. Lett. 139B (1984) 431.

31. P. Minkowski, Phys. Lett. 139B (1984) 431.